Revisiting the Active Sites at the MoS 2 /H 2 O Interface via Grand-Canonical DFT: The Role of Water Dissociation

Nawras Abidi, Audrey Bonduelle-Skrzypczak, Stephan N. Steinmann

Revisiting the Active Sites at the MoS_2/H_2O Interface via Grand-Canonical DFT: The Role of Water Dissociation

Nawras Abidi,[†] Audrey Bonduelle-Skrzypczak,[‡] and Stephan N. Steinmann[*,†]

†*Univ Lyon, Ens de Lyon, CNRS UMR 5182, Universit Claude Bernard Lyon 1, Laboratoire de Chimie, F69342, Lyon, France*

‡*IFP Energies nouvelles, Rond-point de l'échangeur de Solaize, 69360 Solaize, France*

E-mail: stephan.steinmann@ens-lyon.fr

Phone: (+33)4 72 72 81 55

Abstract

MoS_2 is a promising low-cost catalyst for the hydrogen evolution reaction (HER). However, the nature of the active sites remains debated. By taking the electrochemical potential explicitly into account using grand-canonical density functional theory (DFT) in combination with the linearized Poisson-Boltzmann equation, we herein revisit the active sites of 2H-MoS_2. In addition to the well-known catalytically active edge sites, also specific point-defects on the otherwise inert basal plane provide highly active sites for HER. Given that HER takes place in water, we also assess the reactivity of these active sites with respect to H_2O. The thermodynamics of proton reduction as a function of the electrochemical potential reveals that four edge sites and three basal plane defects feature thermodynamic over-potentials below 0.2 V. In contrast to current proposals, many of these active sites involve adsorbed OH. The results demonstrate that even though H_2O and OH block "active" sites, HER can also occur on these "blocked" sites,

reducing protons on surface OH/H_2O entities. As a consequence, our results revise the active sites, highlighting the so far overlooked need to take the liquid component (H_2O) of the functional interface into account when considering the stability and activity of the various active sites.

Keywords

MoS_2, Hydrogen evolution reaction, grand-canonical DFT, water interface, edges, defects, active sites

1 Introduction

Production of clean, renewable and affordable energy is a critical challenge because of the growing population and the current dependence on non-renewable fossil fuels, which produce green-house gases when converted into energy.[1,2] Among the possible alternative energy resources, dihydrogen (H_2, which we simply call hydrogen in the following) has the advantages of emitting only water during the combustion process and having the highest mass energy density.[3,4] Electrocatalytic water splitting is proposed as the most convenient and promising method to produce H_2.[5,6] Pt is the most active and stable known hydrogen evolution reaction (HER) catalyst,[7] with an experimental over-potential of ≈ 0 V and a small Tafel slope, in particular in acidic conditions.[8] Despite that it is not the limiting element for water splitting electrolysers when compared to Ir used as electrocatalyst for OER,[9] the high cost of Pt contributes to the economic barrier towards the large-scale implementation of HER for clean H_2 production. Therefore, developing active and stable electrocatalysts composed of earth abundant materials to replace the expensive platinum-group metals would make a significant step toward turning hydrogen into a competitive energy vector.[10,11]

The family of 2D materials is believed to provide powerful candidates to catalyze the HER. Among the newly discovered catalysts belonging to this family, the transition metal

carbides, nitrides, and carbonitrides, MXenes, have been predicted by theory and confirmed experimentally to be active and stable catalysts for the HER in acid solution.[12–14] MXenes have been employed successfully in a large variety of electrochemical applications by reason to their high electronic conductivity and optimal adsorption strength for key reaction intermediates.[15,16]

Another 2D material that has drawn significant attention in recent years and which is the subject of our study is molybdenum disulfide. Although MoS_2 and its hydrogen-adsorption energy was already well studied,[17] it was only the work of Hinnemann et al.[18] that changed the perception of MoS_2 as being inactive for HER, since their DFT computations predicted that MoS_2 would be a promising alternative to Pt for HER. Soon after, Chorkendorff and co-authors[19] experimentally confirmed that MoS_2 shows promising HER characteristics. Since then, the development of MoS_2-based HER catalysts serves as an excellent example of theory-guided discovery and design of electrocatalysts.[20]

This combination between experimental techniques and density functional theory (DFT) computations has been key to gain detailed insight into the activity and mechanisms of the functional electrochemical MoS_2 interface.[21,22] Depending on the coordination of Mo atoms within a single layer and the stacking order of the layers, three polytypes of MoS_2 are distinguished: 1T, 2H and 3R.[23] 2H-MoS_2 is the most stable polymorph in acid and alkaline solutions,[24,25] while 1T can only be stabilized under specific conditions such as intercalation.[26] Therefore, we will only study the 2H-MoS_2/water interface herein.

Several studies demonstrate that the basal plane and the edges of this material present different electrocatalytic properties. In fact, the pristine basal plane is inert and the edges are highly active.[27] This was confirmed experimentally by finding that the rate of HER reaction is directly proportional to the number of edge sites, regardless of the particle size.[19] Furthermore, several strategies have been developed in order to enhance the HER activity of MoS_2 edges. One strategy focuses on improving the intrinsic activity of the edges by maximally exposing edge sites using nanostructured MoS_2 like nanowires,[28] nanoparticles[29]

or mesoporous films,[30] sometimes in interaction with active supports such as CoS_2.[31] Another strategy strives to ameliorate the edge sites through chemical doping.[32]

Conductivity has also been pointed out as a key aspect of MoS_2 electrocatalytic interfaces.[33] In particular, the edge sites provide both, active sites and enhance the conductivity due to metallic edge-states. Furthermore, there are also active sites on the basal plane, which provide catalytic activity if the electrons do not have to travel too far before reaching the conductive support. In other words, controlling and minimizing the number of stacked layers increases the activity of MoS_2.[34]

Defects generally play an important role in the diversification of the properties of two-dimensional materials and in particular for the activity of the MoS_2 interface.[6] A joint experimental and theoretical study has shown that the dominant defects in experimentally available MoS_2 are the sulfur vacancies V_S, di-vacancies V_{S2}, the anti-site Mo_S with molybdenum replacing sulfur and Mo_{S2} or Mo_{S2*} which are anti sites in combination with S vacancy.[35] Even though the formation energies of these defects is positive, the relative abundance of Mo and S during the synthesis of MoS_2 allows to tune the relative amounts of the defects due to kinetic reasons. For example, mechanical exfoliation was found to mainly feature sulfur vacancy defects, while physical vapor deposition lead to a dominance of Mo_S anti-site defects.[35] Several groups have shown that the 2H-MoS_2 basal plane is activated by V_S defects. It was further demonstrated that elastic strain can be used to tune ΔG_H, so that $\Delta G_H = 0$ in 2H-MoS_2 could be achieved under certain conditions. Reassuringly, these insights are fully compatible with the corresponding experimental findings.[34,36,37]

It has also been demonstrated that a number of single transition metal atom dopants (TM) can be chemisorbed on the basal plane of monolayer 2H-MoS_2 in order to enhance the HER activity.[38–41] Moreover, Zn doping not only reduces the Svacancy formation energy, but has also a beneficial effect on nearby active sites for HER. Previous studies have, however, shown that defects created on the edges of molybdenum disulfide do not increase the activity for HER.[42,43]

The computational method employed to measure the catalyst performance is the Gibbs free energy. Based on the Sabatier principle of heterogeneous catalysis, an optimal activity can be achieved when we have a thermoneutral value of the adsorption energy of a hydrogen atom, i.e., $\Delta G_H \approx 0$ eV.[44] A very positive value indicates that the intermediates bind too weakly and it is difficult for the surface to activate them, but a very negative value signifies that they bind too strongly. In this case, the desorption of the products is hindered and the catalyst is poisoned.[45] Accordingly, one typically obtains a volcano diagram with the highest current density and an intermediate adsorption energy, where Pt is positioned.[19]

To better understand the details of HER the electrified MoS_2 interface immersed in the electrolyte solution needs to be simulated. We herein apply the computationally efficient grand-canonical DFT approach[46–48] and investigate the competition with adsorption of the water solvent. In contrast to the computational hydrogen electrode (CHE) method,[49] grand-canonicl DFT allows to explicitly take the polarization of the electrode into account, thus going beyond the purely thermodynamic effects of the electrochemical potential on the energy of proton/electron pairs. In our approach, the electrode and adsorbates, as well as the surface charge which tunes the electrochemical potential are described via DFT while the electrolyte and solvent are represented by the solution of the linearized Poisson-Boltzmann (PB) equation.[50,51] Previously, we have successfully applied this approach not only to the characterization of the electrochemical interface,[52,53] but also to the elucidation of reaction mechanisms at electrified interfaces such as the oxygen evolution reaction on CoOOH[54] or on iron doped graphenes[55] and even for the electrochemical promotion of catalysis,[56,57] demonstrating its great versatility.

In this article we first highlight additional, experimentally observed, defects on the MoS_2 basal plane that could serve as active sites. Then we move to the importance of considering the different components of the functional electrocatalytic interface, which includes water. Indeed, despite the progress in the study of MoS_2, nothing is known regarding the nature of the active sites in the presence of water. Therefore, we not only probe the adsorption

of H as a function of the electrochemical potential as is frequently done[5] but also H_2O and electrochemically generated surface *OH. This analysis reveals that some of the active sites discussed in the literature are blocked by H_2O, while on others water is not strongly adsorbed. More intriguingly, on a third category H_2O water is strongly adsorbed, but might be directly involved in HER, a possibility that has been overlooked so far.

2 Methods

2.1 Computational details

The first principles computations are performed using the periodic DFT code called "Vienna ab initio simulation package", VASP.[58] We adopted the PBE-dDsC[59,60] density functional, which belongs to the family of the Generalized Gradient Approximation (GGA) and is supplemented with a density-dependent dispersion correction.[61] The nuclei and core electrons are described by the the projector augmented wave function (PAW)[62,63] approach. A plane-wave basis set with a kinetic energy cutoff of 500 eV is utilized for the valence electrons. The precision setting of VASP is set to accurate. The Brillouin zone is integrated by a Monkhorst-Pack k-points mesh. For the description of our p(4×4) surfaces, we choose $1 \times 1 \times 1$ for the basal planes, $3 \times 3 \times 1$ for the edges and for the bulk (2x2x1) cell we work with $5 \times 5 \times 5$. The convergence criterion for the self-consistency process is set to 10^{-5} eV for the optimization of the wave function. The maximum forces are converged to 0.025 eV/ during the geometry optimization. Approximately 15 Å of vacuum is added both above and below the slabs in the z-direction.[61] All geometries and unit cells are given in the supporting information.

The electrochemical interface is described by the solution of the linearized Poisson-Boltzmann equation as implemented in VASPsol.[51] In VASPsol, the interface is defined as a function of the electron density, which is compared to a "critical" density, ρ_c. The default value of ρ_c has been optimized against solvation energies of small molecules in water.[64] However, applying these settings leads to a significant polarization density, i.e., presence of

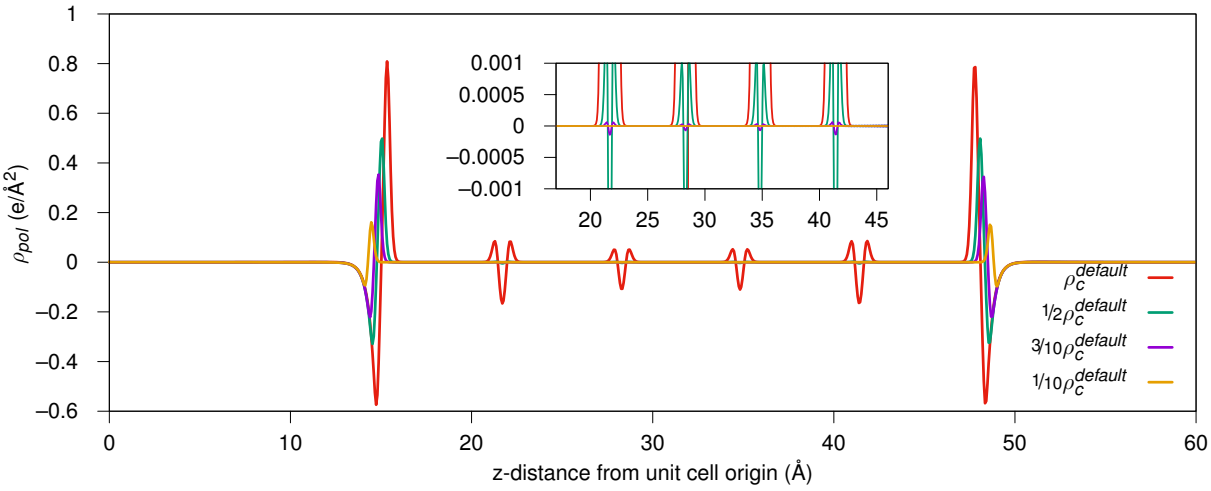

Figure 1: Evolution of the polarization density as a function of the distance between the different layers in the studied system. The inset shows zoom on the region between the MoS_2 sheets.

solvent, between the dispersion bound MoS_2 layers as shown in Fig. 1. Therefore, we have gradually reduced ρ_c in order to identify an iso-density value that completely excludes water between the layers. The final choice is 0.00025 $e^-/\text{Å}^{-1}$, which corresponds to one tenth of the default value. This makes the DFT computations slower than usual due to the larger numerical noise but it allows us to remove the solvent between different layers and it has previously been used in the context of solvated alkali-metal ions.[65,66] The Debey screening length is set to 3 Å, corresponding to a 1 M electrolyte.

In order to properly define the workfunction (electrochemical potential) of the interface, the dipole moment of the slab needs to be nullified through symmetry. For basal planes, we perform symmetrization with respect to a plane, whereas for the edges, we realize a point symmetrization. The central layers are kept frozen in their bulk positions. Fig. 2 shows two typical examples for the obtained unit cells.

2.2 Potential dependence of the energy

As detailed in our previous work, the potential dependence is studied by adapting the surface charge.[54,56] In practice, the charge of the system is varied from -1 to +1 in steps of 0.2 e^-. The

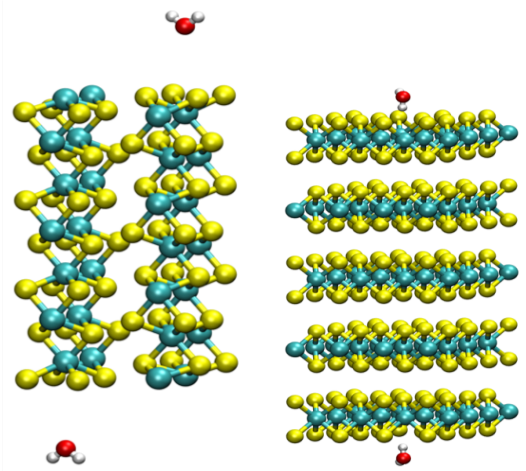

(a) (b)

Figure 2: The structure of H_2O adsorption on polytype 2H after symmetrization (a) on the edge, (b) on the basal plane. The color code for atoms is white for H; red for O; yellow for S and greenish for Mo.

obtained relationship between the grand-canonical energy and the electrochemical potential is then fitted to an analytical formula, which is a parabola for conductors. This is performed in full analogy to the double-reference method of Filhol and Neurock,[67] and is much more flexible than the use of explict cations[49,68,69] since non-integer numbers of electrons allow to fine-tune the surface charge and can be neutralized via the Poisson-Boltzmann equation. Such a fine-tuning is particularly valuable for MoS_2, which can be a conductor or a semi-conductor, depending on the surface (state). Note that we assume large MoS_2 flakes, i.e. we have converged the results with respect to the system size. For smaller nanoflakes, the band-gap opens, just like in other two-dimenstional materials.[70] Such finite size effects are beyond the scope of this study.

In Fig. 3 we show the relative grand-canonical energy with respect to the neutral slab for two systems Mo_{S2} and H@Mo_{S2}, as a function of the electrochemical potential. In H@Mo_{S2} hydrogen is adsorbed on the anti-site defect which is combined with a sulfur vacancy. This leads to a typical conductor, where the energy as a function of the potential can be fitted by a parabola (see Fig. 3a). However, in the absence of adsorption, Mo_{S2} is a semi-conductor, just like bulk MoS_2. This is clearly seen in Fig. 3b, where the energy is constant within

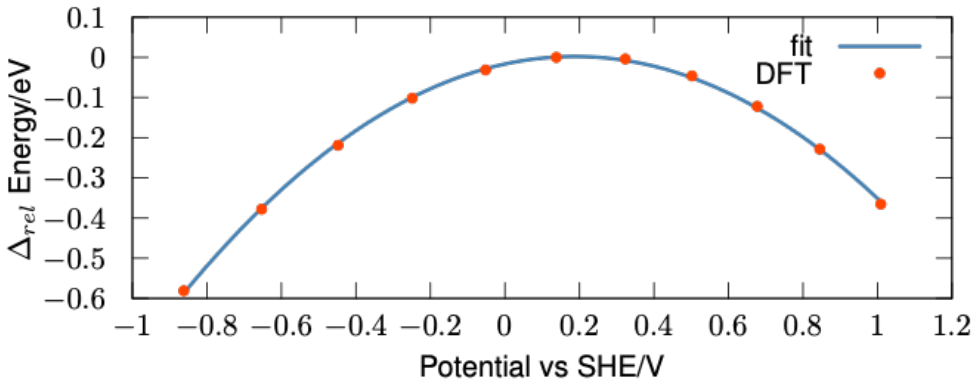

(a) Conductor

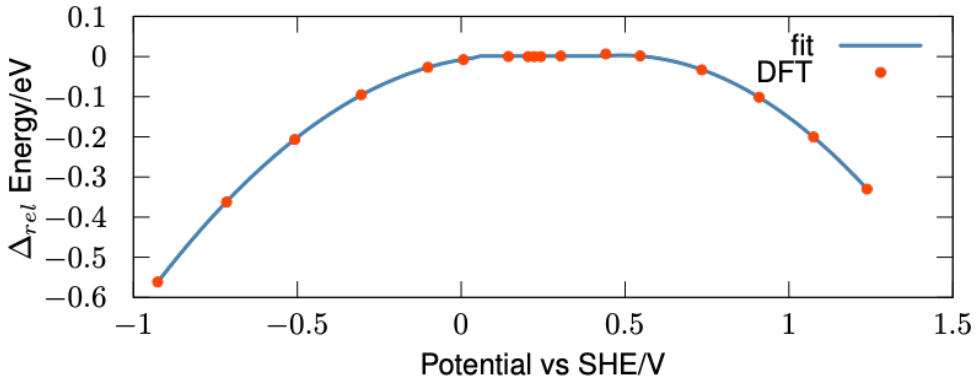

(b) Semi-conductor

Figure 3: Variation of the total energy as a function of the electrochemical potential (a) H@Mo_{S2} and (b) Mo_{S2} with respect to the energy of the neutral slab.

the gap, i.e., from 0.05 V to 0.45 V. Both cases can, however, be described conveniently with analytical formulas to obtain a continuous description of the energy as a function of the potential.

2.3 Adsorption energy

For isolated molecules we use the following approximation for their free energy:

$$G_{mol} = E_{mol} - TS \tag{1}$$

where T is room temperature (298.15 K), and S is the contribution of rotational translational entropy at standard pressure. For water, this entropy contribution is divided by two to account for its liquid state.[71,72]

The adsorption energy ΔG_{ads} of the different species are calculated according to the following formula:[73]

$$G_{ads}(U) = \frac{1}{2} \times (E_{tot}(U) - E_{slab}(U) - R) \tag{2}$$

Where $E_{tot}(U)$ and $E_{slab}(U)$ are the potential dependent energies of the symmetric MoS_2 surface with and without adsorbates, respectively. If the adsorbate is hydrogen (i.e., one hydrogen atom per surface), the reactant (R) will be defined as below:

$$R = 2 \times (H^+ + e^-) = 2\mu_H(U) = G_{H_{2(g)}} - 2eU \tag{3}$$

With G_{H_2} is the free energy of the hydrogen molecule, e is the number of electrons and U is the applied potential with respect to the standard hydrogen electrode. As pointed out by Norskov and co-workers, the chemical potential of protons and electrons can be conveniently replaced by that of hydrogen molecules and the energy correction for the electron due to the electrode potential.[49] In the general case, Equation 3 includes a pH dependence. However, since we here assess HER in acidic conditions, we assume a pH of 0 for which Eq. 3 is directly

applicable. For the adsorption of the water molecule, R = $2G_{H_2O}$. For OH adsorption under the relevant reducing conditions we set $R = 2G_{H_2O}+2(H^+ + e^-) - 2G_{H_2}$. In other words, *OH is created by adsorption of H_2O with a subsequent electroreduction (formally a Heyrovsky step) that liberates H_2. Accordingly, the adsorbed *OH and H_2O species, can also lead to the formation of H_2 (see Figure 4). Note, that this surface OH* is not to be identified with OH^- adsorption: First, it originates from the dissociation of H_2O and can, therefore, even in acidic conditions be present at the interface. Second, its generation is linked to water reduction ($H_2O + H^+ + e^- \longrightarrow \cdot OH + H_2$, so that it formally should be considered as an adsorbed hydroxyl "radical" and not an adsorbed hydroxide "ion".

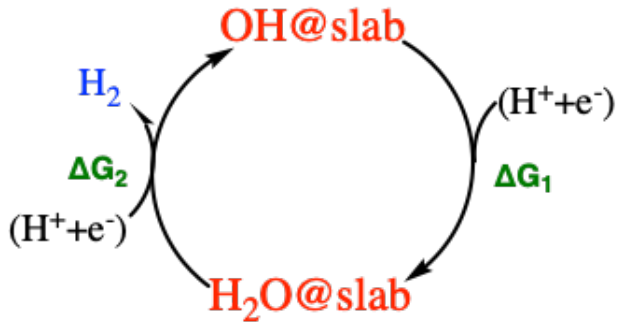

Figure 4: H_2 evolution via H_2O and OH. ΔG_1 corresponds to a Volmer step (adsorption of $H^+ + e-$), while ΔG_2 is a Heyrovsky step.

When a second adsorbate is adsorbed, the adsorption energy is computed just like for the first one, except that the initial surface already contains one adsorbate. To be explicit, the second adsorption energy is neither the sum nor the average adsorption energy, but the differential adsorption energy.

For a successful HER catalyst, the ΔGs must be as close to zero as possible. They are calculated according to the following formulas:

$$\Delta G_1 = \frac{1}{2} \times (E_{tot}(\mathrm{H_2O}) - E_{tot}(\mathrm{OH}) - 2 \times (\mathrm{H^+ + e^-})) \tag{4}$$

$$\Delta G_2 = \frac{1}{2} \times (E_{tot}(\mathrm{OH}) + 2 \times G_{\mathrm{H_2}} - E_{tot}(\mathrm{H_2O}) - 2 \times (\mathrm{H^+ + e^-})) \tag{5}$$

3 Results and discussion

3.1 Basal plane

Using a descriptor-based analysis with the hydrogen adsorption free energy, the perfect basal plane was showed previously to be catalytically inert[18,19] and our computations with an applied electrochemical potential leeds to the same conclusion (see Fig. S1 in the supporting information). Hence, we focus in this part of our work on the basal plane with the different possible defects cited before.

3.1.1 Active sites for HER

In order to identify the active sites for HER, various defects at the 2H-MoS_2 basal plane interface are investigated. The hydrogen adsorption energy ΔG_H was first computed in vacuum for an extensive list of defects (see Fig. S2 in the supporting information). The most promising ones are the commonly investigated sulfur (di-)vacancies (V_S and V_{S2}), the anti-site (Mo_S) and the anti-site with sulfur vacancies (Mo_{S2}) that have not been considered in the literature (see Fig. 5). For these sites, the potential dependent $\Delta G_H(U)$ in strongly acidic conditions (pH 0) are computed according to Eq. 2 and 3. In agreement with H adsorption being the Volmer step, $\Delta G_H(U)$ in eV decreases with a near unity slope when moving to ever more reducing potentials in V (see Fig. S3). Compared to the ΔG_H values obtained for adsorption of the hydrogen onto the pristine 2H-MoS_2 basal plane (ΔG $\approx$ 1.67 eV at 0 V), the potential dependent computations confirm that these defects have a binding energy for hydrogen that is compatible with HER. For V_S and V_{S2} a second hydrogen atom can be adsorbed with an adsorption energy close to 0 around 0 V, which opens the possibility for the Volmer-Tafel reaction mechanism on these sites. The most relevant adsorption energies at 0 V are thus summarized in Fig. 5.

We can conclude that the best HER active sites on the basal plane of 2H-MoS_2 are obtained when the molybdenum atom is exposed at the catalyst/solution interface. This

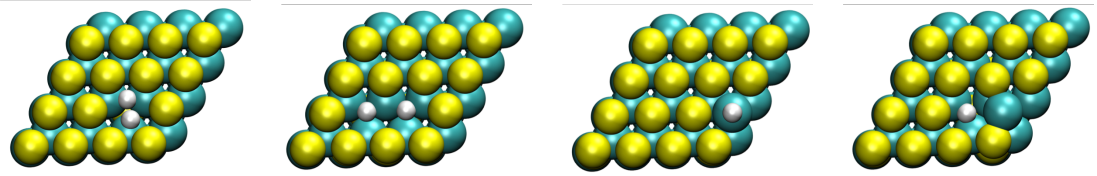

(a) 0.11 eV (b) -0.34 eV (c) -0.06 eV (d) -0.21 eV

Figure 5: Adsorption of hydrogen at 0 V vs SHE on: (a) V_S, (b) V_{S2}, (c) Mo_S, (d) Mo_{S2} The color code for atoms is white for H; yellow for S and greenish for Mo.

can be achieved via sulfur vacancies[5] but also by substituting S by Mo in anti-site defects as demonstrated herein.

3.1.2 Solvent adsorption at the functional interface

The presence of water at the electrochemical interface can have profound impacts on the activity beyond the macroscopic effects that are captured by the Poisson-Boltzmann equation. Therefore, we adsorb water molecules on the different defects at the MoS_2 interface (see Figure 6). Note that the adsorption of a water molecule is formally a chemical step. Therefore, in comparison to the adsorption of $H^+ + e^-$, the adsorption energy of H_2O depends much less on the electrochemical potential. Nevertheless, the surface dipole moment of H_2O@MoS_2 leads to a non-negligible potential dependence due to its interaction with the potential-generated electric field.[52] As shown in the SI, ΔG is roughly decreasing in the case of Mo_S and Mo_{S2*S} sites and increasing for V_S and V_{S2} with the increase of the electrochemical potential (see Fig. S4). Sulfur vacancies and anti-sites behave, however, very differently: V_S and V_{S2} feature nearly thermoneutral ΔG_{H_2O} (0.05 eV and 0.04 eV respectively), while H_2O binds very strongly on Mo_S and Mo'_{S2} (-0.92 eV and -0.80 eV respectively), where the $'$ indicates that the adsorbate is located on the anti-site Mo atom. Hence, H_2O at the electrochemical interface might block HER active sites for Mo_S and Mo'_{S2}, while water is more weakly interacting with the vacancies.

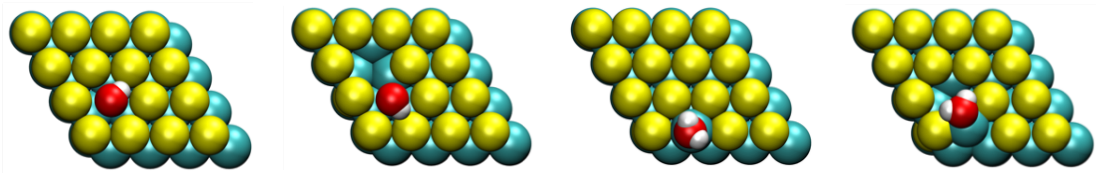

(a) 0.05 eV (b) 0.04 eV (c) -0.92 eV (d) -0.80 eV

Figure 6: Adsorption of water at 0 V vs SHE on: (a) V_S, (b) V_{S2}, (c) Mo_S, (d) Mo'_{S2} The color code for atoms is white for H; red for O; yellow for S and greenish for Mo.

3.1.3 Production of H_2 from adsorbed OH and H_2O

Given the propensity of water adsorption on active sites, we assess the possibility of HER to occur via a H_2O/OH cycle (see Fig. 4). As shown in the SI, *OH formation is exothermic at the relevant potentials (see Fig. S5), suggesting that it can be obtained under HER conditions via a Heyrovsky step, generating H_2, which is denoted as ΔG_2 (Eq. 5). The surface OH can then be reduced back to H_2O via a Volmer step with a reaction energy ΔG_1 (Eq. 4). We note in passing, that this generation of (formally neutral) adsorbed OH* is not equivalent to the adsorption of (formally charged) OH^-. Hence, the thermodynamics of the electrochemical OH* formation is not expected to be strongly dependent on the pH, but mostly a function of the electrochemical potential. Furthermore, at oxidizing potentials, OH* can also be formed via oxidation, rather than reduction, i.e., via $H_2O \longrightarrow \cdot OH + e^- + H^+$, which contrasts with our case defined in section 2.3. This alternative pathway for OH* formation is also the reason why our results cannot be directly transposed to hydrogen oxidation reaction conditions, where positive potentials instead of the negative ones are relevant.

To probe the effectiveness of the different active sites, we adopt the notion of a thermodynamic overpotential η_{TD}.[49] This is the minimal potential that needs to be applied in addition to the Nernst potential (0 V vs SHE for HER at pH 0) in order to drive the electrochemical reaction. It is determined as the potential that allows to form each reaction intermediate via a thermoneutral or exothermic step. We report η_{TD} in Table 1, together with ΔG_1 and ΔG_2. Furthermore, we illustrate the catalytic cycle for the most promising site, Mo_S, in

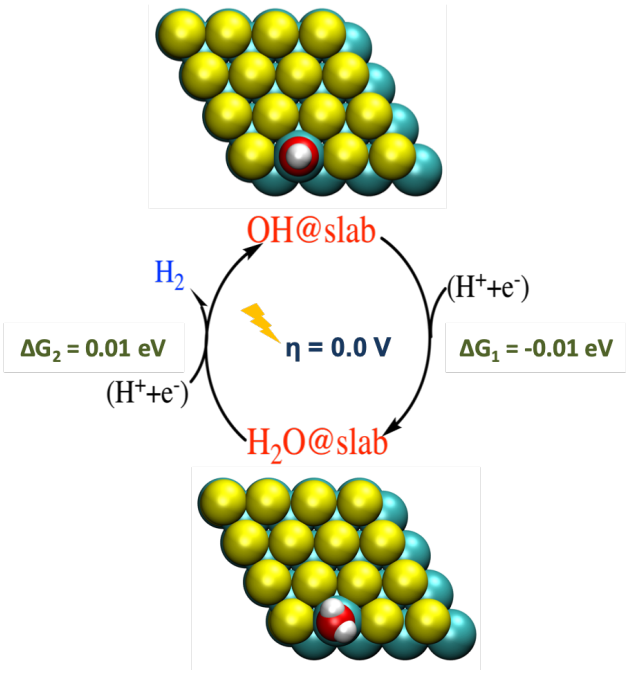

Figure 7: Different steps of the first cycle to produce H_2 from H_2O and OH on Mo_S site The color code for atoms is white for H; red for O; yellow for S and greenish for Mo.

Fig. 7. Indeed, Mo_S remains an active site even though H_2O is strongly adsorbed: both of the ΔGs are very close to 0 eV at zero potential. Similarly, on Mo'_{S2} the Heyrovsky step (ΔG_2) to produce H_2 only requires an over-potential of 0.3 V, so that this site is also active for HER at the aqueous interface.

Table 1: Thermodynamic overpotentials η_{TD} and corresponding reaction energies for HER via OH/H_2O cycling.

Type of defect	ΔG_1 (eV)	ΔG_2 (eV)	η_{TD} (V)
Mo_S	-0.01	0.01	0.0
Mo'_{S2}	0.01	-0.61	0.3
V_S	0.03	-0.83	0.4
V_{S2}	0.05	-1.65	0.8

For the vacancies, water is weakly adsorbed and from Table 1 the overpotential for HER is high (0.4 V V_S and 0.8 V for V_{S2}) due to ΔG_1, i.e., the Volmer step. In other words, H_2O is not stable enough with respect to OH on the surface. However, since H_2O is not strongly bound, the vacancies could remain "empty" and evolve H_2 without the direct participation of water.

To summarize, all the defects presented are active sites for HER without H_2O. If H_2O is adsorbed on Mo'_{S2} or Mo_S the sites remain thermodynamically very effective via a Volmer-Heyrovsky mechanism involving *OH. Note that these sites have a significant abundance in MoS_2 produced by physical vapor deposition.[35] In contrast, water covered V_S and V_{S2} sites are inactive for HER. However, since H_2O is barely adsorbed on the vacancies, we suggest that these active sites might not be hindered too much and remain active even at the solid/liquid interface. In order to identify the precise reaction mechanism (Volmer-Tafel or Volmer-Heyrovsky) on these vacancy sites, potential dependent reaction barriers for the Tafel and Heyrovsky steps would need to be determined, which is beyond the scope of this study.

3.2 HER on edges sites and the influence of water adsorption

While the basal plane is the most exposed surface, except for defects, it has no catalytic activity. This is in stark contrast with the minority edges sites of MoS_2, which are known to be active sites. The study that is most closely connected to ours is the work by Goddard and co-workers:[22] They have performed an in-depths kinetic and thermodynamic study of the HER at the half-sulfided edge of MoS_2 at the grand-canonical density functional theory level. Furthermore, they have even investigated the transition states for the relevant reaction steps. As shown and discussed in the supporting information, our level of theory is in full agreement with previous reports (see Fig. S6), i.e., the edges are predicted to be highly active.

Since the edges are, however, also exposed to the water solvent at the catalytic interface, we investigate the adsorption energy of H_2O as a function of the electrochemical potential. Here, we show only the most stable configurations (see Fig. 8), while in the SI we also report other arrangements tested. According to the Fig S7, the first water molecule adsorbed is strongly bonded to the Mo-edge and only weakly on the S edge at 0 V. For the S-edge, water adsorption becomes, however, more exothermic when going to more reducing potentials.

Note that we here consider the Mo-edge of the stoichiometric MoS_2 slabs. The exposure of Mo atoms, rather than partially sulfided edges, might be relevant for HER conditions, where the production of H_2 can also lead to the irreversible desorption of H_2S, which contrasts with the traditionally studied gas-phase hydro-desulfurization conditions.[74,75] Hence, we decided to investigate the two "extreme" cases (Mo-edge and S-edge), rather than half-sulfided edges, which have been investigated by Goddard and co-workers.[22] Of course, the actual composition of the active edge sites might have various stoichiometries and even be varying over time. However, an in-depth study of the activation energies and dissolution of H_2S under HER conditions is beyond the scope of this study. Since the first H_2O molecule seems well adsorbed and the catalytic interface is immersed in water, we assess the energetics for the adsorption of a second molecule. For both edges, the second water molecule is more strongly adsorbed, last but not least due to the hydrogen bond created with the first one (see Fig. S8). However, just like the S-vacancies, the S-edge interacts only weakly with water. Assessing the formation of *OH on the edge sites (see Fig. S10), demonstrates that for the Mo edge *OH outcompetes hydrogen, while the S-edge binds OH only very weakly. As a consequence, it does not come as a surprise that HER involving OH/H_2O on the S-edge features high thermodynamic overpotentials (see Table 2). However, the S-edge might remain barely affected by water, i.e., remain active for HER, but without the direct implication of water.

Having established that the Mo-edge is likely covered with H_2O and OH under realistic conditions, we now return to the question of HER on these active sites. Figure 9 shows an energy profile at 0.2 V, which is lower than the 0.5 V given in Table 2 for η_{TD}. At this potential, the Heyrovsky step, producing H_2 and adsorbed OH is exothermic. At this point, HER can further proceed either via a Volmer step, regenerating the water molecule or, via a second Heyrovsky step, leading to two OHs on the edge. The former reaction step is endothermic at this potential, while the latter is athermic. Hence, the system is more likely to move to 2 OH on the edge. Once this intermediate reached, even at only 0.2 V, the Volmer step is exothermic, so that HER is successfully achieved by cycling between OH and

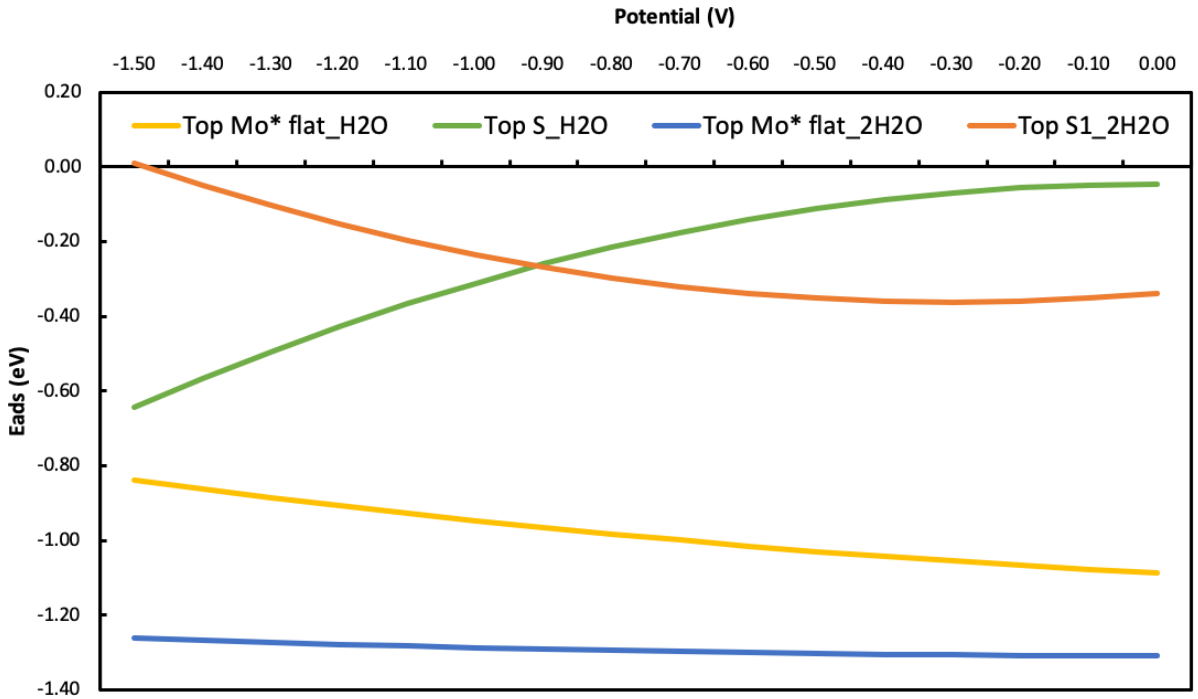

(a) Variation of the adsorption energy of the water molecule on the different edge sites as a function of the electrochemical potential.

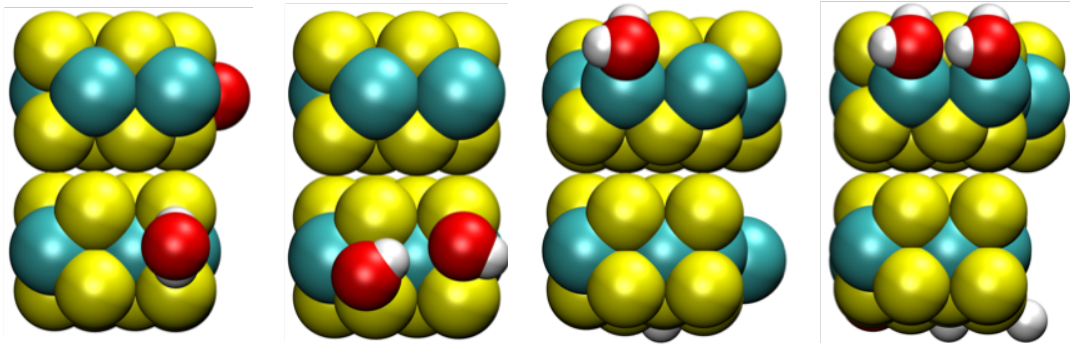

(b) Top S H_2O (c) Top S1 $2H_2O$ (d) Top Mo*flat H_2O (e) Top Mo*flat $2H_2O$

Figure 8: The adsorption energies of water on Mo and S edges with the the optimized geometry of each site. The color code for atoms is white for H; red for O; yellow for S and greenish for Mo.

H_2O with a co-adsorbed OH.

Table 2: The over-potential applied to produce H_2

Type of site	ΔG_1 (eV)	ΔG_2 (eV)	η_{TD} (V)
Top S2	-1.84	0.04	1.3
Top Mo* flat	0.02	-1.02	0.5

To conclude, the Mo-edge forms strong bonds with water. HER can, nevertheless, take place with a thermodynamic overpotential of only 0.2 V involving OH/H_2O cycling at the aqueous MoS_2 interface.

Our results, demonstrating possible activity for OH* covered MoS_2 active sites, might also be in line with the relative stable (tens to hundreds of hours) performances of MoS_2 type catalysts in strongly alkaline media,[34,76,77] where OH* formation is expected to be (kinetically) even more pronounced.

4 Conclusion

We have investigated the thermodynamics of the hydrogen evolution reaction at the interface of 2H-MoS_2 with an aqueous electrolyte applying grand-canonical DFT to take the effect of the electrochemical potential explicitly into account. Our computations identify four promising point-defects on the basal plane in addition to the well-known active sites on the edges of this 2D material. Since under reaction conditions water is necessarily present, we have also carefully studied the influence of the adsorption of H_2O molecules and their dissociation into adsorbed OH, a competition that has been overlooked so far. H_2O does not interact strongly with the sulfur edges and the sulfur vacancies on the basal plane. Hence, these sites can be considered unaffected by the presence of water. In contrast, the anti-site defects and the Mo-edges are clearly covered with OH and H_2O. Intriguingly, this does, however, not completely deactivate this sites, as a Volmer-Heyrovsky mechanism involving cycling between adsorbed OH and H_2O still allows for HER with very low (< 0.2 V) thermodynamic overpotentials. This computational prediction could eventually be probed

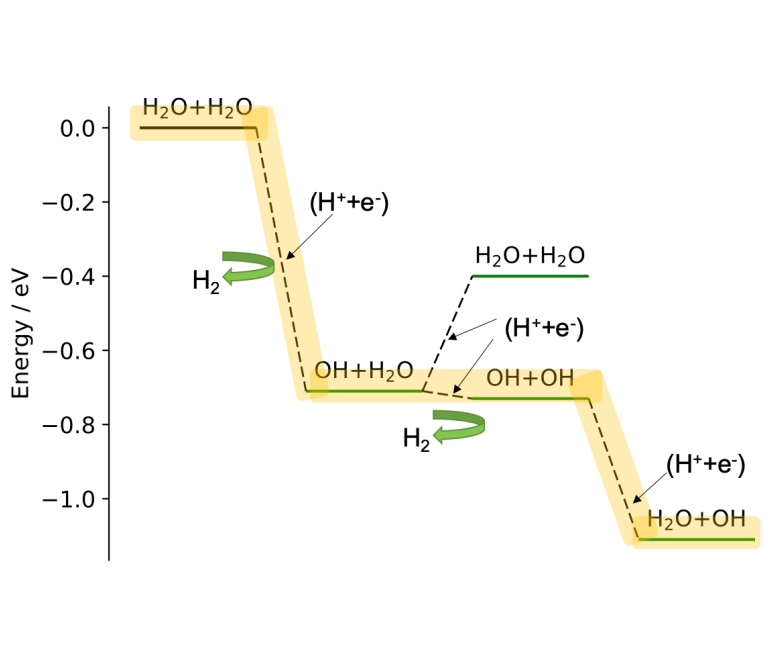

(a) Reaction energy profile at 0.2 V

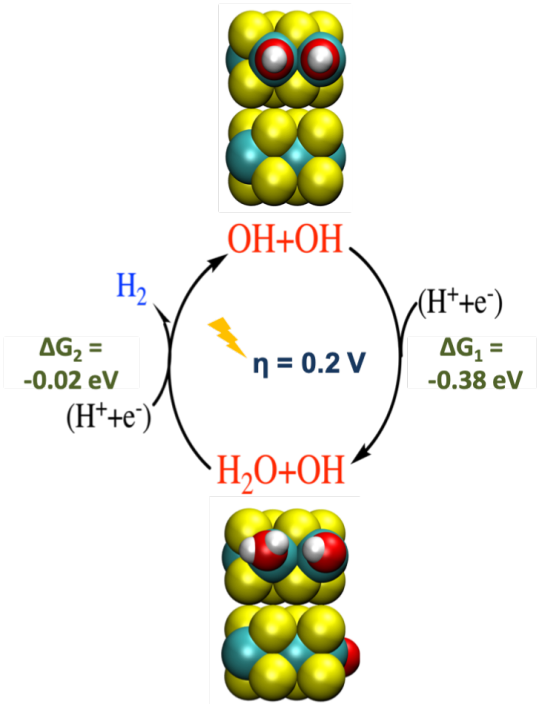

(b) Catalytic cycle

Figure 9: Production of H_2 on the OH covered Mo-edge, involving OH and H_2O. The thermodynamic overpotential η_{TD} is determined to be 0.2 V. In the reaction energy profile (a) the thermodynamically feasible pathway starting with adsorbed water molecules is highlighted in yellow. The first step is initiating the thermodynamic cycle, which is then depicted in (b). The color code for atoms is white for H; red for O; yellow for S and greenish for Mo.

experimentally, as the presence of chemisorbed oxygen species on the MoS_2 could be identified and quantified, for instance via operando-XPS or NMR studies. Furthermore, defective MoS_2 with anti-sites or partially oxidized edges would, according to our findings, still show a significant HER activity. In summary, our findings highlight the necessity to include all major consituents of the solid/liquid interface in order achieve an atomistic understanding of the reactivity.

Acknowledgement

This work was financially supported by Région Auvergne Rhône-Alpes through the project Pack Ambition Recherche 2018 MoSHi. We are very grateful to IFP Energies nouvelles for supporting the MoSHy project (N^o 1801167601) and to the IFP Energies nouvelles team, Mona Marie Obadia and Quentin Cacciuttolo, for discussing the MoS_2 solids that should meet the predictions of molecular modeling in the case of hydrogen production by water electrolysis. The authors thank the SYSPROD project and AXELERA Pôle de Compétitivité for financial support (PSMN Data Center).

Supporting Information Available

The supplementary material contains additional Figures and Tables, as well as the coordinates of all symmetric zero-charge systems investigated herein. A short discussion of the relative stability of the MoS_2 polytypes is also provided.

This material is available free of charge via the Internet at `http://pubs.acs.org/`.

References

(1) Greeley, J.; Jaramillo, T. F.; Bonde, J.; Chorkendorff, I.; Nørskov, J. K. Computational high-throughput screening of electrocatalytic materials for hydrogen evolution. *Nature*

Materials **2006**, *5*, 909–913.

(2) Solangi, K. H.; Islam, M. R.; Saidur, R.; Rahim, N. A.; Fayaz, H. A review on global solar energy policy. *Renewable and Sustainable Energy Reviews* **2011**, *15*, 2149–2163.

(3) Kibler, L. A. Hydrogen electrocatalysis. *ChemPhysChem* **2006**, *7*, 985–991.

(4) Fan, X. L.; Yang, Y.; Xiao, P.; Lau, W. M. Site-specific catalytic activity in exfoliated MoS2 single-layer polytypes for hydrogen evolution: Basal plane and edges. *Journal of Materials Chemistry A* **2014**, *2*, 20545–20551.

(5) Kronberg, R.; Hakala, M.; Holmberg, N.; Laasonen, K. Hydrogen adsorption on MoS2-surfaces: A DFT study on preferential sites and the effect of sulfur and hydrogen coverage. *Physical Chemistry Chemical Physics* **2017**, *19*, 16231–16241.

(6) Ye, G.; Gong, Y.; Lin, J.; Li, B.; He, Y.; Pantelides, S. T.; Zhou, W.; Vajtai, R.; Ajayan, P. M. Defects Engineered Monolayer MoS2 for Improved Hydrogen Evolution Reaction. *Nano Letters* **2016**, *16*, 1097–1103.

(7) Trasatti, S. Work function, electronegativity, and electrochemical behaviour of metals: III. Electrolytic hydrogen evolution in acid solutions. *Journal of Electroanalytical Chemistry and Interfacial Electrochemistry* **1972**, *39*, 163–184.

(8) Luo, W.; Gan, J.; Huang, Z.; Chen, W.; Qian, G.; Zhou, X.; Duan, X. Boosting HER Performance of Pt-based Catalysts Immobilized on Functionalized Vulcan Carbon by Atomic Layer Deposition. *Frontiers in Materials* **2019**, *6*, 251.

(9) Kibsgaard, J.; Chorkendorff, I. Considerations for the scaling-up of water splitting catalysts. *Nature Energy* **2019**, *4*, 430.

(10) Ding, Q.; Song, B.; Xu, P.; Jin, S. Efficient Electrocatalytic and Photoelectrochemical Hydrogen Generation Using MoS2 and Related Compounds. *Chem* **2016**, *1*, 699–726.

(11) Seh, Z. W.; Kibsgaard, J.; Dickens, C. F.; Chorkendorff, I.; Nørskov, J. K.; Jaramillo, T. F. Combining theory and experiment in electrocatalysis: Insights into materials design. *Science* **2017**, *355*, eaad4998.

(12) Seh, Z. W.; Fredrickson, K. D.; Anasori, B.; Kibsgaard, J.; Strickler, A. L.; Lukatskaya, M. R.; Gogotsi, Y.; Jaramillo, T. F.; Vojvodic, A. Two-dimensional molybdenum carbide (MXene) as an efficient electrocatalyst for hydrogen evolution. *ACS Energy Letters* **2016**, *1*, 589–594.

(13) Li, P.; Zhu, J.; Handoko, A. D.; Zhang, R.; Wang, H.; Legut, D.; Wen, X.; Fu, Z.; Seh, Z. W.; Zhang, Q. High-throughput theoretical optimization of the hydrogen evolution reaction on MXenes by transition metal modification. *J. Mater. Chem. A* **2018**, *6*, 4271–4278.

(14) Handoko, A. D.; Fredrickson, K. D.; Anasori, B.; Convey, K. W.; Johnson, L. R.; Gogotsi, Y.; Vojvodic, A.; Seh, Z. W. Tuning the Basal Plane Functionalization of Two-Dimensional Metal Carbides (MXenes) To Control Hydrogen Evolution Activity. *ACS Appl. Energy Mater.* **2018**, *1*, 173–180.

(15) Handoko, A. D.; Steinmann, S. N.; Seh, Z. W. Theory-guided materials design: two-dimensional MXenes in electro- and photocatalysis. *Nanoscale Horiz.* **2019**, *4*, 809–827.

(16) Handoko, A. D.; Steinmann, S. N.; Wei, F.; Seh, Z. W. Correction: Theory-guided materials design: two-dimensional MXenes in electro-and photocatalysis. *Nanoscale Horizons* **2019**, *4*, 1014–1014.

(17) Raybaud, P.; Hafner, J.; Kresse, G.; Kasztelan, S.; Toulhoat, H. Ab Initio Study of the H2–H2S/MoS2 Gas–Solid Interface: The Nature of the Catalytically Active Sites. *Journal of Catalysis* **2000**, *189*, 129–146.

(18) Hinnemann, B.; Moses, P. G.; Bonde, J.; Jørgensen, K. P.; Nielsen, J. H.; Horch, S.; Chorkendorff, I.; Nørskov, J. K. Biomimetic hydrogen evolution: MoS2 nanoparticles

as catalyst for hydrogen evolution. *Journal of the American Chemical Society* **2005**, *127*, 5308–5309.

(19) Jaramillo, T. F.; Jørgensen, K. P.; Bonde, J.; Nielsen, J. H.; Horch, S.; Chorkendorff, I. Identification of active edge sites for electrochemical H2 evolution from MoS2 nanocatalysts. *Science* **2007**, *317*, 100–102.

(20) Benck, J. D.; Hellstern, T. R.; Kibsgaard, J.; Chakthranont, P.; Jaramillo, T. F. Catalyzing the hydrogen evolution reaction (HER) with molybdenum sulfide nanomaterials. *ACS Catalysis* **2014**, *4*, 3957–3971.

(21) Benck, J. D.; Hellstern, T. R.; Kibsgaard, J.; Chakthranont, P.; Jaramillo, T. F. Catalyzing the Hydrogen Evolution Reaction (HER) with Molybdenum Sulfide Nanomaterials. *ACS Catal.* **2014**, *4*, 3957–3971.

(22) Huang, Y.; Nielsen, R. J.; Goddard, W. A. Reaction Mechanism for the Hydrogen Evolution Reaction on the Basal Plane Sulfur Vacancy Site of MoS2 Using Grand Canonical Potential Kinetics. *Journal of the American Chemical Society* **2018**, *140*, 16773–16782.

(23) Song, I.; Park, C.; Choi, H. C. Synthesis and properties of molybdenum disulphide: From bulk to atomic layers. *RSC Advances* **2015**, *5*, 7495–7514.

(24) Enyashin, A. N.; Yadgarov, L.; Houben, L.; Popov, I.; Weidenbach, M.; Tenne, R.; Bar-Sadan, M.; Seifert, G. New route for stabilization of 1T-WS2 and MoS2 phases. *The Journal of Physical Chemistry C* **2011**, *115*, 24586–24591.

(25) Zhao, W.; Pan, J.; Fang, Y.; Che, X.; Wang, D.; Bu, K.; Huang, F. Metastable MoS2 : Crystal Structure, Electronic Band Structure, Synthetic Approach and Intriguing Physical Properties. *Chemistry - A European Journal* **2018**, *24*, 15942–15954.

(26) Lukowski, M. A.; Daniel, A. S.; Meng, F.; Forticaux, A.; Li, L.; Jin, S. Enhanced Hydrogen Evolution Catalysis from Chemically Exfoliated Metallic MoS2 Nanosheets. *J. Am. Chem. Soc.* **2013**, *135*, 10274–10277.

(27) Wilson, J. A.; Yoffe, A. D. The transition metal dichalcogenides discussion and interpretation of the observed optical, electrical and structural properties. *Advances in Physics* **1969**, *18*, 193–335.

(28) Chen, Z.; Cummins, D.; Reinecke, B. N.; Clark, E.; Sunkara, M. K.; Jaramillo, T. F. Core–shell MoO3–MoS2 nanowires for hydrogen evolution: a functional design for electrocatalytic materials. *Nano letters* **2011**, *11*, 4168–4175.

(29) Bonde, J.; Moses, P. G.; Jaramillo, T. F.; Nørskov, J. K.; Chorkendorff, I. Hydrogen evolution on nano-particulate transition metal sulfides. *Faraday discussions* **2009**, *140*, 219–231.

(30) Kibsgaard, J.; Chen, Z.; Reinecke, B. N.; Jaramillo, T. F. Engineering the surface structure of MoS2 to preferentially expose active edge sites for electrocatalysis. *Nature materials* **2012**, *11*, 963–969.

(31) Zuo, X.; Chang, K.; Zhao, J.; Xie, Z.; Tang, H.; Li, B.; Chang, Z. Bubble-template-assisted synthesis of hollow fullerene-like MoS $_2$ nanocages as a lithium ion battery anode material. *J. Mater. Chem. A* **2016**, *4*, 51–58.

(32) Benck, J. D.; Chen, Z.; Kuritzky, L. Y.; Forman, A. J.; Jaramillo, T. F. Amorphous molybdenum sulfide catalysts for electrochemical hydrogen production: insights into the origin of their catalytic activity. *Acs Catalysis* **2012**, *2*, 1916–1923.

(33) Voiry, D.; Salehi, M.; Silva, R.; Fujita, T.; Chen, M.; Asefa, T.; Shenoy, V. B.; Eda, G.; Chhowalla, M. Conducting MoS2 Nanosheets as Catalysts for Hydrogen Evolution Reaction. *Nano Lett.* **2013**, *13*, 6222–6227.

(34) Li, G.; Zhang, D.; Yu, Y.; Huang, S.; Yang, W.; Cao, L. Activating MoS2 for pH-Universal Hydrogen Evolution Catalysis. *Journal of the American Chemical Society* **2017**, *139*, 16194–16200.

(35) Hong, J.; Hu, Z.; Probert, M.; Li, K.; Lv, D.; Yang, X.; Gu, L.; Mao, N.; Feng, Q.; Xie, L.; Zhang, J.; Wu, D.; Zhang, Z.; Jin, C.; Ji, W.; Zhang, X.; Yuan, J.; Zhang, Z. Exploring atomic defects in molybdenum disulphide monolayers. *Nature Communications* **2015**, *6*, 1–8.

(36) Li, G.; Zhang, D.; Qiao, Q.; Yu, Y.; Peterson, D.; Zafar, A.; Kumar, R.; Curtarolo, S.; Hunte, F.; Shannon, S.; Zhu, Y.; Yang, W.; Cao, L. All the Catalytic Active Sites of MoS2 for Hydrogen Evolution. *Journal of the American Chemical Society* **2016**, *138*, 16632–16638.

(37) Ouyang, Y.; Ling, C.; Chen, Q.; Wang, Z.; Shi, L.; Wang, J. Activating inert basal planes of MoS2 for hydrogen evolution reaction through the formation of different intrinsic defects. *Chemistry of Materials* **2016**, *28*, 4390–4396.

(38) Lau, T. H.; Lu, X.; Kulhavỳ, J.; Wu, S.; Lu, L.; Wu, T.-S.; Kato, R.; Foord, J. S.; Soo, Y.-L.; Suenaga, K. Transition metal atom doping of the basal plane of MoS2 monolayer nanosheets for electrochemical hydrogen evolution. *Chemical science* **2018**, *9*, 4769–4776.

(39) Shi, Y.; Zhou, Y.; Yang, D. R.; Xu, W. X.; Wang, C.; Wang, F. B.; Xu, J. J.; Xia, X. H.; Chen, H. Y. Energy Level Engineering of MoS2 by Transition-Metal Doping for Accelerating Hydrogen Evolution Reaction. *Journal of the American Chemical Society* **2017**, *139*, 15479–15485.

(40) Voiry, D.; Yang, J.; Chhowalla, M. Recent strategies for improving the catalytic activity of 2D TMD nanosheets toward the hydrogen evolution reaction. *Advanced Materials* **2016**, *28*, 6197–6206.

(41) Lukowski, M. A.; Daniel, A. S.; Meng, F.; Forticaux, A.; Li, L.; Jin, S. Enhanced hydrogen evolution catalysis from chemically exfoliated metallic MoS2 nanosheets. *Journal of the American Chemical Society* **2013**, *135*, 10274–10277.

(42) Li, H.; Tsai, C.; Koh, A. L.; Cai, L.; Contryman, A. W.; Fragapane, A. H.; Zhao, J.; Han, H. S.; Manoharan, H. C.; Abild-Pedersen, F.; Nørskov, J. K.; Zheng, X. Activating and optimizing MoS2 basal planes for hydrogen evolution through the formation of strained sulphur vacancies. *Nature Materials* **2016**, *15*, 48–53.

(43) Tsai, C.; Li, H.; Park, S.; Park, J.; Han, H. S.; Nørskov, J. K.; Zheng, X.; Abild-Pedersen, F. Electrochemical generation of sulfur vacancies in the basal plane of MoS2 for hydrogen evolution. *Nature communications* **2017**, *8*, 1–8.

(44) Che, M. Nobel Prize in chemistry 1912 to Sabatier: Organic chemistry or catalysis? *Catalysis Today* **2013**, *218*, 162–171.

(45) Medford, A. J.; Vojvodic, A.; Hummelshøj, J. S.; Voss, J.; Abild-Pedersen, F.; Studt, F.; Bligaard, T.; Nilsson, A.; Nørskov, J. K. From the Sabatier principle to a predictive theory of transition-metal heterogeneous catalysis. *Journal of Catalysis* **2015**, *328*, 36–42.

(46) Melander, M. M.; Kuisma, M. J.; Christensen, T. E. K.; Honkala, K. Grand-canonical approach to density functional theory of electrocatalytic systems: Thermodynamics of solid-liquid interfaces at constant ion and electrode potentials. *J. Chem. Phys.* **2018**, *150*, 041706.

(47) Hörmann, N. G.; Andreussi, O.; Marzari, N. Grand canonical simulations of electrochemical interfaces in implicit solvation models. *J. Chem. Phys.* **2019**, *150*, 041730.

(48) Zhang, H.; Goddard, W. A.; Lu, Q.; Cheng, M.-J. The importance of grand-canonical quantum mechanical methods to describe the effect of electrode potential on the sta-

bility of intermediates involved in both electrochemical CO2 reduction and hydrogen evolution. *Phys. Chem. Chem. Phys.* **2018**, *20*, 2549–2557.

(49) Nørskov, J. K.; Rossmeisl, J.; Logadottir, A.; Lindqvist, L.; Kitchin, J. R.; Bligaard, T.; Jonsson, H. Origin of the overpotential for oxygen reduction at a fuel-cell cathode. *The Journal of Physical Chemistry B* **2004**, *108*, 17886–17892.

(50) Mathew, K.; Sundararaman, R.; Letchworth-Weaver, K.; Arias, T.; Hennig, R. G. Implicit solvation model for density-functional study of nanocrystal surfaces and reaction pathways. *The Journal of chemical physics* **2014**, *140*, 084106.

(51) Mathew, K.; Kolluru, V. S. C.; Mula, S.; Steinmann, S. N.; Hennig, R. G. Implicit self-consistent electrolyte model in plane-wave density-functional theory. *J. Chem. Phys.* **2019**, *151*, 234101.

(52) Steinmann, S. N.; Sautet, P. Assessing a First-Principles Model of an Electrochemical Interface by Comparison with Experiment. *The Journal of Physical Chemistry C* **2016**, *120*, 5619–5623.

(53) Fang, Y.; Ding, S.; Zhang, M.; Steinmann, S. N.; Hu, R.; Mao, B.; Feliu, J. M.; Tian, Z. Revisiting the atomistic structures at the interface of Au(111) electrode-sulfuric acid solution. *J. Am. Chem. Soc.* **2020**, *142*, 9439–9446.

(54) Curutchet, A.; Colinet, P.; Michel, C.; Steinmann, S. N.; Le Bahers, T. Two-sites are better than one: revisiting the OER mechanism on CoOOH by DFT with electrode polarization. *Physical Chemistry Chemical Physics* **2020**, *22*, 7031–7038.

(55) Shang, R.; Steinmann, S. N.; Xu, B.-Q.; Sautet, P. Mononuclear Fe in N-doped carbon: computational elucidation of active sites for electrochemical oxygen reduction and oxygen evolution reactions. *Catal. Sci. Technol.* **2020**, *10*, 1006–1014.

(56) Hajar, Y. M.; Treps, L.; Michel, C.; Baranova, E. A.; Steinmann, S. N. Theoretical insight into the origin of the electrochemical promotion of ethylene oxidation on ruthenium oxide. *Catalysis Science and Technology* **2019**, *9*, 5915–5926.

(57) Panaritis, C.; Michel, C.; Couillard, M.; Baranova, E. A.; Steinmann, S. N. Elucidating the role of electrochemical polarization on the selectivity of the CO2 hydrogenation reaction over Ru. *Electrochimica Acta* **2020**, *350*, 136405.

(58) Kresse, G.; Furthmüller, J. Efficiency of ab-initio total energy calculations for metals and semiconductors using a plane-wave basis set. *Computational Materials Science* **1996**, *6*, 15–50.

(59) Perdew, J. P.; Burke, K.; Ernzerhof, M. Generalized Gradient Approximation Made Simple. *Physical review letters* **1996**, *77*, 3865.

(60) Steinmann, S. N.; Corminboeuf, C. Comprehensive Benchmarking of a Density-Dependent Dispersion Correction. *Journal of Chemical Theory and Computation* **2011**, *7*, 3567–3577.

(61) Steinmann, S. N.; Sautet, P.; Michel, C. Solvation free energies for periodic surfaces: comparison of implicit and explicit solvation models. *Physical Chemistry Chemical Physics* **2016**, *18*, 31850–31861.

(62) Blochl, P. E. Projector augmented-wave method. *Phys. Rev. B* **1994**, *50*, 17953.

(63) Kresse, G.; Joubert, D. From ultrasoft pseudopotentials to the projector augmented-wave method. *Phys. Rev. B* **1999**, *59*, 1758.

(64) Letchworth-Weaver, K.; Arias, T. A. Joint density functional theory of the electrode-electrolyte interface: Application to fixed electrode potentials, interfacial capacitances, and potentials of zero charge. *Phys. Rev. B* **2012**, *86*, 075140.

(65) Steinmann, S. N.; Michel, C.; Schwiedernoch, R.; Sautet, P. Impacts of electrode potentials and solvents on the electroreduction of CO2: A comparison of theoretical approaches. *Physical Chemistry Chemical Physics* **2015**, *17*, 13949–13963.

(66) Lespes, N.; Filhol, J. S. Using Implicit Solvent in Ab Initio Electrochemical Modeling: Investigating Li+/Li Electrochemistry at a Li/Solvent Interface. *Journal of Chemical Theory and Computation* **2015**, *11*, 3375–3382.

(67) Taylor, C. D.; Wasileski, S. A.; Filhol, J.-S.; Neurock, M. First principles reaction modeling of the electrochemical interface: Consideration and calculation of a tunable surface potential from atomic and electronic structure. *Physical Review B* **2006**, *73*, 165402.

(68) Mukherjee, J.; Linic, S. First-principles investigations of electrochemical oxidation of hydrogen at solid oxide fuel cell operating conditions. *Journal of The Electrochemical Society* **2007**, *154*, B919–B924.

(69) Ingram, D. B.; Linic, S. First-principles analysis of the activity of transition and noble metals in the direct utilization of hydrocarbon fuels at solid oxide fuel cell operating conditions. *Journal of the Electrochemical Society* **2009**, *156*, B1457–B1465.

(70) Li, X.; Melissen, S. T. A. G.; Le Bahers, T.; Sautet, P.; Masters, A. F.; Steinmann, S. N.; Maschmeyer, T. Shining Light on Carbon Nitrides: Leveraging Temperature To Understand Optical Gap Variations. *Chem. Mater.* **2018**, *30*, 4253–4262.

(71) Deubel, D. V.; Lau, J. K.-c. In silico evolution of substrate selectivity : comparison of organometallic ruthenium complexes with the anticancer drug cisplatin . **2006**, *2*, 2451–2453.

(72) Kua, J.; Thrush, K. L. HCN, Formamidic Acid, and Formamide in Aqueous Solution: A Free-Energy Map. *J. Phys. Chem. B* **2016**, *120*, 8175–8185.

(73) He, H.; Lu, P.; Wu, L.; Zhang, C.; Song, Y.; Guan, P.; Wang, S. Structural Properties and Phase Transition of Na Adsorption on Monolayer MoS2. *Nanoscale Research Letters* **2016**, *11*, 330.

(74) Badawi, M.; Paul, J.; Cristol, S.; Payen, E.; Romero, Y.; Richard, F.; Brunet, S.; Lambert, D.; Portier, X.; Popov, A.; Kondratieva, E.; Goupil, J.; El Fallah, J.; Gilson, J.; Mariey, L.; Travert, A.; Maugé, F. Effect of water on the stability of Mo and CoMo hydrodeoxygenation catalysts: A combined experimental and DFT study. *Journal of Catalysis* **2011**, *282*, 155–164.

(75) Prodhomme, P. Y.; Raybaud, P.; Toulhoat, H. Free-energy profiles along reduction pathways of MoS2 M-edge and S-edge by dihydrogen: A first-principles study. *Journal of Catalysis* **2011**, *280*, 178–195.

(76) Ren, B.; Li, D.; Jin, Q.; Cui, H.; Wang, C. Integrated 3D self-supported Ni decorated MoO2 nanowires as highly efficient electrocatalysts for ultra-highly stable and large-current-density hydrogen evolution. *J. Mater. Chem. A* **2017**, *5*, 24453–24461.

(77) Sun, T.; Wang, J.; Chi, X.; Lin, Y.; Chen, Z.; Ling, X.; Qiu, C.; Xu, Y.; Song, L.; Chen, W.; Su, C. Engineering the Electronic Structure of MoS2 Nanorods by N and Mn Dopants for Ultra-Efficient Hydrogen Production. *ACS Catalysis* **2018**, *8*, 7585–7592.

Graphical TOC Entry